PNAS RESEARCH ARTICLE | CELL BIOLOGY OPEN ACCESS

Adaptive exchange sustains cullin–RING ubiquitin ligase networks and proper licensing of DNA replication

Yaru Zhang[a], Marco Jost[b,c,d,1], Ryan A. Pak[b,c,d,2], Daniel Lu[e], Jing Li[a], Brett Lomenick[f], Spiros D. Garbis[f,3], Chi-Ming Li[e], Jonathan S. Weissman[b,c,d,4], James Russell Lipford[a], and Raymond J. Deshaies[g,h,5]

Contributed by Raymond Deshaies; received April 6, 2022; accepted June 24, 2022; reviewed by Jean Cook and Michele Pagano

Cop9 signalosome (CSN) regulates the function of cullin–RING E3 ubiquitin ligases (CRLs) by deconjugating the ubiquitin-like protein NEDD8 from the cullin subunit. To understand the physiological impact of CSN function on the CRL network and cell proliferation, we combined quantitative mass spectrometry and genome-wide CRISPR interference (CRISPRi) and CRISPR activation (CRISPRa) screens to identify factors that modulate cell viability upon inhibition of CSN by the small molecule CSN5i-3. CRL components and regulators strongly modulated the antiproliferative effects of CSN5i-3, and in addition we found two pathways involved in genome integrity, SCF^{FBXO5}–APC/C–GMNN and $CUL4^{DTL}$–SETD8, that contribute substantially to the toxicity of CSN inhibition. Our data highlight the importance of CSN-mediated NEDD8 deconjugation and adaptive exchange of CRL substrate receptors in sustaining CRL function and suggest approaches for leveraging CSN inhibition for the treatment of cancer.

Cop9 signalosome | CSN5i-3 | CRISPR screen | DNA replication | deneddylation

Cullin•RING ubiquitin ligases (CRLs) comprise a large family of enzymes implicated in many aspects of cellular and organismal physiology (1–3). There are eight human cullins (CUL1-3, CUL4A/B, CUL5, CUL7, and CUL9), each of which interacts with a RING protein (RBX1 or RBX2) and a set of substrate receptor (SR)•adaptor complexes. Together these complexes constitute a family of at least 250 E3 ubiquitin ligases and direct ~20% of proteasome-mediated protein degradation (4). A key mechanism that regulates all known CRLs is conjugation of the ubiquitin-like protein NEDD8 to a conserved lysine residue in cullins (5, 6), which recruits the co-E3 ARIH1 (7) and causes a profound conformational change in the CRL resulting in enhanced ubiquitin transfer to substrate (8, 9). Multiple E2 enzymes have been implicated in CRL-dependent ubiquitination, including the ARIH1-binding E2 UBE2L3/UBCH7 and the RBX1/2-binding E2s UBE2D3/UBCH5C, UBE2R1/CDC34A, UBE2R2/CDC34B, and UBE2G1 (10–13).

Cullin neddylation is catalyzed by NEDD8-activating enzyme (NAE) (APPBP1•UBA3), E2-conjugating enzyme (UBE2M/UBC12 and UBE2F), and E3 ligase (DCUN1D1–DCUN1D5) (14–18). Pevonedistat (MLN4924) is a small molecule inhibitor of NAE (4) and is currently being explored in multiple clinical trials. Pevonedistat inhibits neddylation, and thus is thought to inactivate all CRLs. The NEDD8 modification is transient and reversed by the COP9 signalosome (CSN) isopeptidase (19, 20). Human CSN is a heteromeric complex of nine subunits, CSN1 to CSN9 (21, 22). Although CSN-mediated NEDD8 deconjugation inhibits CRLs in vitro, genetic studies show that CSN is a positive regulator of CRLs in vivo (23). The best explanation for this discrepancy is that in the absence of CSN activity, constitutively activated CRLs induce autoubiquitination and degradation of their SR subunits (24, 25). Functionally, CSN is essential for development, and knockout of different CSN subunits in mouse is embryonic lethal (26). Recently, Schlierf et al. (27) identified CSN5i-3 as a potent and selective inhibitor of CSN. CSN5i-3 caused depletion of several CRL substrate receptors, possibly via autoubiquitylation.

Cellular studies of pevonedistat demonstrated that the CRL substrate CDT1 is stabilized as a result of SCF^{SKP2} and $CRL4^{DTL}$ inactivation (28, 29). CDT1 is a DNA replication licensing factor required for prereplication complex (pre-RC) assembly (30). Initiation of DNA replication is a tightly controlled process, in which CDT1 cooperates with CDC6 and the origin recognition complex (ORC) to promote the loading of MCM2-7 (minichromosome maintenance) complex onto DNA to generate a pre-RC (30). GMNN (Geminin) inhibits DNA replication by sequestering CDT1 (31). After initiation of DNA replication is triggered by CDK2 and DBF4•CDC7, CDT1 is degraded, GMNN accumulates, and CDC6 is exported from the nucleus, thus preventing refiring of the origin (30). CDT1 stabilization caused by pevonedistat leads to DNA rereplication, accumulation of cells in S phase, and eventual cell death (28, 29).

Significance

The deneddylase Cop9 signalosome (CSN) regulates the function of cullin-RING ubiquitin ligases (CRLs), which are involved in regulating myriad cellular functions through the ubiquitin-mediated degradation of proteins such as transcription factors, cell cycle regulators, and signal transduction proteins. CSN inhibition by the small molecule inhibitor, CSN5i-3, has differential effects on CRL function. Some CRLs are profoundly inactivated when CSN is inhibited, whereas others are barely affected. Therefore, it is difficult to deconvolute the effects of CSN inhibition on cells. To untangle this, we used CRISPRi and CRISPRa screens and identified two contributing pathways involved in DNA replication licensing. The knowledge can potentially be used to guide selection of cancer patients that are most likely to respond to CSN5i-3.

Reviewers: J.C., The University of North Carolina at Chapel Hill; and M.P., HHMI and NYU School of Medicine.

[1]Present address: Department of Microbiology, Harvard Medical School, Boston, MA 02115.

[2]Present address: Department of Neuroscience, The Scripps Research Institute, La Jolla, CA 92037.

[3]Present address: Proteas Bioanalytics Inc., Torrance, CA 90502.

[4]Present address: Whitehead Institute for Biomedical Research, Massachusetts Institute of Technology, Cambridge, MA 02139.

[5]To whom correspondence may be addressed. Email: rdii2003@gmail.com.

This article contains supporting information online at http://www.pnas.org/lookup/suppl/doi:10.1073/pnas.2205608119/-/DCSupplemental.

Published August 29, 2022.

In prior work we reported that the cellular composition of CUL1-based CRL complexes is controlled by a process we dubbed "adaptive exchange" (*SI Appendix*, Fig. S1*A*), wherein the assembly state of a particular SCF/CRL1 substrate receptor is determined by the abundance of its substrates (32). We postulated that this control is mediated by NEDD8, coupled with the activity of the substrate receptor exchange factor CAND1 (33). According to this model, a CRL complex is conjugated with NEDD8 upon its formation. In the presence of the substrate, deconjugation of NEDD8 is impeded because the substrate interferes with CSN binding (34–36). Once the substrate is depleted, CSN deconjugates NEDD8, which enables CAND1 to bind and catalyze exchange of the assembled SR•adaptor module for one from the cell's pool of excess unassembled modules. Three key lines of evidence supported this model. First, when conjugation of NEDD8 is blocked by pevonedistat, there is a strong reduction in assembled SCF complexes at the expense of CUL1•CAND1 complexes (37). Second, knockout of *CAND1* and *CAND2* results in increased assembly of most SCF complexes (37). Third, stimuli that generate substrates for particular SCF or CRL4 complexes increase the steady-state level of those complexes (32, 37–39).

A key prediction of the adaptive exchange hypothesis is that maintenance of a functional network of CRL complexes should depend on both NEDD8 conjugation and deconjugation. In the absence of NEDD8 deconjugation, cells are predicted to accumulate CRL complexes for which there are no substrates. These should persist, due to negligible dissociation of SR•adaptor modules from cullins, until the unoccupied SR is turned over via autoubiquitylation. The discovery of CSN5i-3 allowed us to test this prediction with CRL4, where we were able to show that brief CSN inhibition leads to increased assembly of most CRL4 complexes (39). Here, we employ mass spectrometry and CRISPR screens to evaluate the proteome-wide physical and functional impact of CSN inhibition. Our findings support the central tenets of the adaptive exchange hypothesis and identify biology that is perturbed upon CSN inhibition, including licensing of DNA replication and maintenance of genome integrity. Deregulation of these pathways upon exposure to CSN5i-3 creates a heightened vulnerability to DNA damage checkpoint inhibitors that could potentially be exploited in cancer therapy.

Results

CSN5i-3 Is an Uncompetitive Inhibitor of Cop9 Signalosome. We first set out to characterize the biochemical and pharmacological properties of CSN5i-3 (Fig. 1*A*). CSN5i-3 is a potent and specific inhibitor of CSN, with a half maximal inhibitory concentration (IC_{50}) of ∼5.4 nM in a deneddylation reaction with purified NEDD8–CRL4 (27). Unexpectedly, CSN5i-3 inhibited CSN uncompetitively when either NEDD8–SCF^{SKP2} or NEDD8–CRL2 were used as substrates (Fig. 1*B* and *SI Appendix*, Fig. S1 *B* and *C*). Titration of CSN5i-3 on K562 and 293T cells yielded a half maximal effective concentration (EC_{50}) of ∼50 nM for deneddylation of all cullins tested (Fig. 1*C* and *SI Appendix*, Fig. S1*D*). Interestingly, CSN5i-3, though noncovalent, was, like the covalent NAE inhibitor pevonedistat, poorly reversible (Fig. 1*D*). Together with the data showing that CSN5i-3 was an uncompetitive inhibitor, this suggests that CSN5i-3, especially in conjunction with proteasome inhibitors, may be a useful tool for stabilizing CRL and CRL•substrate complexes (39).

CSN5i-3 Induces Selective Degradation of CRL Substrate Receptors. CSN5i-3 induces degradation of multiple CRL substrate receptors (27, 38). To investigate the impact of CSN5i-3 on a proteome-wide level, we performed quantitative proteomic mass spectrometry (MS2) by 16-plex isobaric tandom mass tag (TMT) labeling of K562 cells treated with dimethyl sulfoxide (DMSO) or 1 μM CSN5i-3 for 2, 8, and 24 h. Approximately 6,200 proteins were identified, of which 5,063 were quantified. After 24 h, multiple proteins were down-regulated (212) or up-regulated (129) by CSN5i-3 using a cutoff of $|\log_2$ fold change$|>0.3$ and adjusted P values of <0.05 (*SI Appendix*, Fig. S1*E* and Dataset S1). Gene ontology (GO) analysis of these 341 modulated proteins showed enrichment of CSN subunits and cell cycle and chromosome-related proteins (*SI Appendix*, Fig. S1*F*). Strikingly, the top 20 most decreased proteins included 8 CRL adaptors or SRs, 2 CRL E2s, and 2 CSN subunits (Fig. 1*E*). In addition, of the 212 down-regulated proteins, 23 were CRL components or regulators (*SI Appendix*, Fig. S1*G*) and 8 were CSN subunits (*SI Appendix*, Fig. S1*H*). Western blot confirmed a CSN5i-3–dependent decrease in CSN5 (Fig. 1*D*). RNA sequencing (RNA-seq) analysis (*SI Appendix*, Fig. S1*I* and Dataset S2) suggested that these effects were posttranscriptional (Fig. 1*E* and *SI Appendix*, Fig. S1*H*). In contrast, 8 of the top 20 most-increased proteins were reported CRL substrates (Fig. 1*F*) that mapped to cell division–related processes (*SI Appendix*, Fig. S1*F*), and most of the changes were posttranscriptional (Fig. 1*F*).

Overall, proteomics analysis indicated that CSN inhibition with CSN5i-3 led to decreased levels of multiple CRL components and increased levels of multiple CRL substrates. Together, these observations suggest that CSN activity is crucial to maintain CRL activity, even though CSN inhibits CRLs by removing the activating NEDD8 modification, and in short-term exposures stabilizes CRL complexes (39). This seemingly contradictory behavior, known as the "CSN paradox," has been noted previously for particular CRLs (25, 27). Our proteome-wide analysis, along with that of Mayor-Ruiz et al. (38), suggested that a positive role for CSN in sustaining SR abundance and CRL function is a prominent and widespread phenomenon affecting multiple CRLs.

Genome-Wide CRISPR Interference and CRISPR Activation Screens Using CSN5i-3 and Pevonedistat. To extend our analysis of CSN's impact on the CRL network, we addressed whether the changes in protein levels observed in cells treated with CSN5i-3 corresponded to a functional decline in CRL pathway activity. We also sought to identify the most prominent vulnerabilities experienced by cells with diminished CSN activity. We addressed these questions by performing genome-wide CRISPR interference (CRISPRi) and CRISPR activation (CRISPRa) screens to identify modifiers of CSN5i-3 cytotoxicity. K562 cells expressing dCas9-KRAB (for CRISPRi-mediated gene repression) or dCas-SunTag and scFv-VP64 (for CRISPRa-mediated gene induction) were infected with the hCRISPRi-v2 and hCRISPRa-v2 libraries that target 18,905 and 18,915 genes, respectively (Fig. 2*A*) (40–42). After harvesting a t_0 sample, we repeatedly pulsed the remaining cells (at a coverage of >1,000 cells/sgRNA) with DMSO or 1 μM CSN5i-3 for 24 h on indicated days (*SI Appendix*, Fig. S2*A*). After 15 to 17 d (t_{end}) of growth, we measured the relative abundance of sgRNAs in the t_0 and t_{end} DMSO and CSN5i-3 samples by deep sequencing to reveal how each sgRNA affected growth in the absence (t_{end} DMSO vs. t_0, γ) and presence (t_{end} CSN5i-3 vs. t_{end} DMSO, ρ) of the drug (43). Negative and positive γ-values indicate an sgRNA inhibited or promoted growth, respectively, whereas negative and positive ρ-values indicate a sgRNA sensitized to or conferred resistance to CSN5i-3, respectively. CSN5i-3 sensitivity phenotypes of targeted genes were correlated in biological

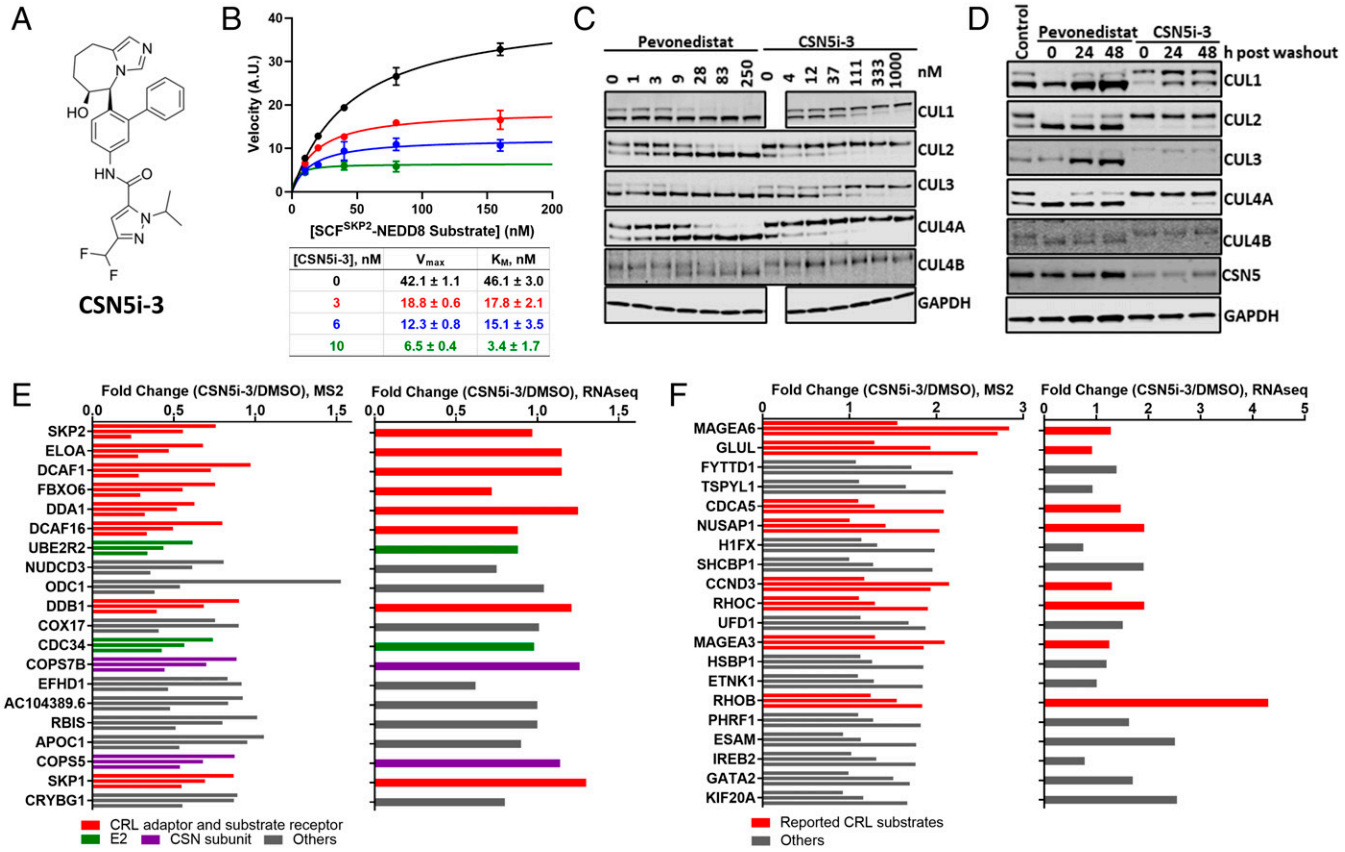

Fig. 1. CSN5i-3 is an uncompetitive inhibitor of CSN and results in degradation of CRL substrate receptors. (*A*) Chemical structure of CSN5i-3. (*B*) CSN5i-3 is an uncompetitive inhibitor of CSN. Assays were conducted at 0.033 nM CSN. Error bars represent ±SD; $n = 3$. (*C*) CSN5i-3 promotes accumulation of NEDD8-conjugated cullins. K562 cells were treated with indicated amounts of pevonedistat or CSN5i-3 for 4 h and immunoblotted to detect the indicated cullins and GAPDH. Representative Western blots are shown; $n = 3$. (*D*) CSN5i-3 is poorly reversible. K562 cells were treated with 1 μM pevonedistat or 1 μM CSN5i-3 for 24 h, washed, and either harvested for analysis (0) or cultured for an additional 24 to 48 h, after which cullins were evaluated as in *C*. Control represents untreated cells. Representative Western blots are shown; $n = 3$. (*E*) Top 20 proteins down-regulated by CSN5i-3. K562 cells were treated with 1 μM CSN5i-3 for 2, 8, or 24 h and proteins in whole cell lysate were quantified by mass spectrometry (MS2). The three bars for each protein represent CSN5i-3 treatment for 2, 8, and 24 h (*Top* to *Bottom*). CRL adaptors and substrate receptors (red), Ub E2s for CRL (green), and CSN subunits (purple) are highlighted. Relative normalized expression of mRNA encoding the corresponding proteins in cells treated with CSN5i-3 vs. DMSO were determined by RNA-seq and are shown on the *Right*. $n = 4$ (MS2) or 2 (RNA-seq). (*F*) Proteins up-regulated by CSN5i-3. This is the same as in *E* except that the top 20 up-regulated proteins are shown. CRL substrate proteins are highlighted in red.

replicates (for genes with $|\rho| > 0.15$ in either replicate, CRISPRi Pearson $r^2 = 0.31$, CRISPRa Pearson $r^2 = 0.47$), whereas those of negative control genes sampled from nontargeting control sgRNAs were clustered around zero (Fig. 2*B*). Although the CRISPRi screen showed more variability than the CRISPRa screen at the level of individual sgRNAs (*SI Appendix*, Fig. S2 *B* and *C*), grouping CRISPR constructs that target the same gene reduced variation and clearly identified genes whose repression consistently altered sensitivity to CSN5i-3 (Fig. 2*B* and *SI Appendix*, Fig. S2 *D* and *E*).

The averaged CRISPRi and CRISPRa phenotypes for all genes are plotted in Fig. 2*C* (Dataset S3). Genes were classified as hits using a combined threshold based on phenotype strength and *P* value (the absolute value of $-\log_{10}(P \text{ value}) \times$ phenotype z-score). Using cutoff values of 20 and 7, the resulting gene-level phenotypes revealed 334 and 262 genes for which repression and induction strongly affects CSN5i-3 sensitivity, respectively (Dataset S3). The CRISPRi screen enriched for genes involved in diverse aspects of proteostasis, as well as in DNA replication, cell cycle regulation, and RNA degradation (*SI Appendix*, Fig. S2*F*). This was underscored by the top 30 genes whose repression conferred sensitivity to CSN5i-3 (Fig. 2*D*). Notably, 7 of these hits were CRL subunits or regulators. CRISPRi constructs for all CSN subunits resulted in sensitization to CSN5i-3, whereas CRISPRa constructs for individual subunits had no effect, consistent with CSN working as an obligate holoenzyme (Fig. 2*C* and *SI Appendix*, Fig. S2*G*). In contrast, hits from the CRISPRa screen were enriched for genes involved in the TGF-β signaling pathway, cancer, cellular senescence, ubiquitin-mediated proteolysis, and osteoclast differentiation (*SI Appendix*, Fig. S2*F*). Again, the top 30 sensitizing hits enriched for CRL subunits or cofactors (Fig. 2*D*). The list of genes from the CRISPRi and CRISPRa screens that yielded the strongest resistance to CSN5i-3 lacked a coherent signature and primarily contained genes involved in transcription regulation, signal transduction, and metabolism, suggesting that these genes may affect CSN5i-3 sensitivity indirectly, potentially through nonspecific effects on cell cycle progression (*SI Appendix*, Fig. S2 *H–J*). Overall, striking enrichment for genes involved in CRL homeostasis suggested that our CRISPR screens successfully captured genetic determinants of CSN5i-3 response.

To orthogonally identify additional factors that regulate the CRL network, we also carried out a CRISPRi screen with the extensively studied NAE inhibitor pevonedistat (*SI Appendix*, Fig. S3 *A* and *B*) (44–47). Pevonedistat has a pervasive inhibitory effect on the assembly of SCF complexes (37) and CRL function (4, 48–50). Consistent with its covalent mechanism of action, pevonedistat elicited widespread, poorly reversible loss of NEDD8–cullin

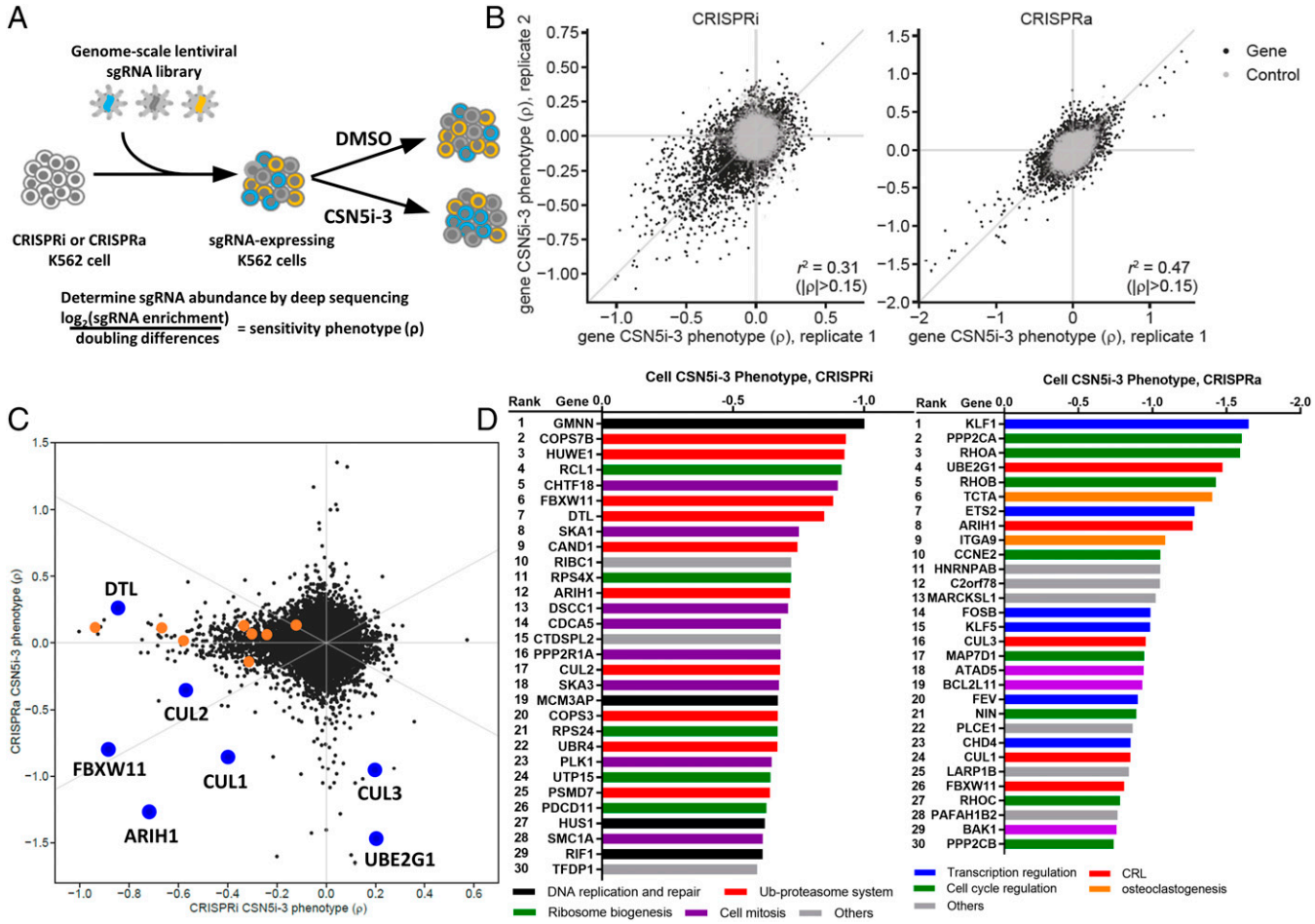

Fig. 2. Genome-wide CRISPRi and CRISPRa screens. (*A*) Schematic of CSN5i-3 sensitivity screens and equation for calculation of sensitivity phenotypes (ρ). Doubling differences refer to differences in population doublings between untreated and treated populations. (*B*) CSN5i-3 sensitivity phenotypes (ρ) for all genes from two biological replicates ($n = 2$) of genome-scale CRISPRi and CRISPRa screens. The ρ-value for each gene was calculated using the average of the top three scoring sgRNAs by absolute value. Negative control genes were generated from nontargeting control sgRNAs. For the CRISPRa screen, sensitivity phenotypes were calculated relative to the same untreated population. (*C*) CRISPRi and CRISPRa CSN5i-3 sensitivity phenotypes of all genes. Phenotype values are the average of two biological replicates ($n = 2$) from *B*. CSN subunits are highlighted in orange. Some CRL genes with strong phenotypes are in blue. (*D*) Genes from the CRISPRi (*Left*) and CRISPRa (*Right*) screens that yielded most enhanced sensitivity to CSN5i-3. Genes are ranked by their sensitivity phenotypes (ρ) and color coded according to cellular pathways; $n = 2$.

conjugates in K562 and 293T cells (Fig. 1 *C* and *D* and *SI Appendix*, Fig. S1*D*). The set of genes whose CRISPRi-mediated repression sensitized cells to pevonedistat was enriched for CRL subunits and regulators (5 of the top 30 sensitizing hits), 4 of which were also identified in the CSN5i-3 screen (Dataset S4 and *SI Appendix*, Fig. S3 *C*–*G*). This reinforces the conclusion that both conjugation and deconjugation of NEDD8 are required to sustain CRL enzyme networks. Notably, repression of several CSN subunits conferred resistance, while repression of several neddylation pathway genes conferred sensitivity to pevonedistat (*SI Appendix*, Fig. S3*D*), consistent with the opposing effects of these enzymes on NEDD8 conjugation.

Genetic Validation of the CSN5i-3 Screen Results. To experimentally validate the results from our CSN5i-3 CRISPR screens, we selected the top one to two sgRNAs for a set of target genes and evaluated their impact on growth in direct competition coculture assays in the presence and absence of CSN5i-3. We selected genes from the CRISPRi (Fig. 3*A* and *SI Appendix*, Fig. S4*A*) and CRISPRa (*SI Appendix*, Fig. S4*B*) screens that enhanced sensitivity to CSN5i-3. For a subset of CRISPRi hits, we also confirmed reductions in mRNA (Fig. 3*B*) and protein levels (*SI Appendix*, Fig. S4*C*). In addition, we tested genes that conferred resistance to CSN5i-3 in the CRISPRi screen (*SI Appendix*, Fig. S4*D*). Overall, the results were in close agreement with the findings of our genome-wide CRISPR screens.

Having validated the general performance of the screens, we next examined the results to understand the physiological impact of CSN inhibition. We first examined genes of the NEDD8 system, followed by the proteasome and other CRL pathway proteins. CRISPRi of CSN subunits rendered cells sensitive to CSN5i-3 (*SI Appendix*, Fig. S2*G*). Conversely, CRISPRi of *DCUN1D1* but not other NEDD8 conjugation factors protected cells from CSN5i-3, suggesting that *DCUN1D1* plays a major role in NEDD8 conjugation (*SI Appendix*, Fig. S4*E*). In contrast, CRISPRi of CSN subunits induced sensitivity (*SI Appendix*, Fig. S3 *C* and *D*). Meanwhile, CRISPRi of the deneddylation-dependent exchange factor *CAND1* was strongly sensitizing to both CSN5i-3 and pevonedistat (*SI Appendix*, Figs. S3 *C* and *D* and S4*E*). This likely represents a synthetic lethality, wherein partial reductions in sequentially acting NEDD8 conjugation/deconjugation and CAND1 forecloses adaptive exchange of substrate receptors.

The observed sensitization upon repression of proteasome subunits and CRL components suggested that cells treated with CSN5i-3 were deficient in CRL–proteasome function (Fig. 3 *C* and *D*). Investigation of the phenotypes of individual genes,

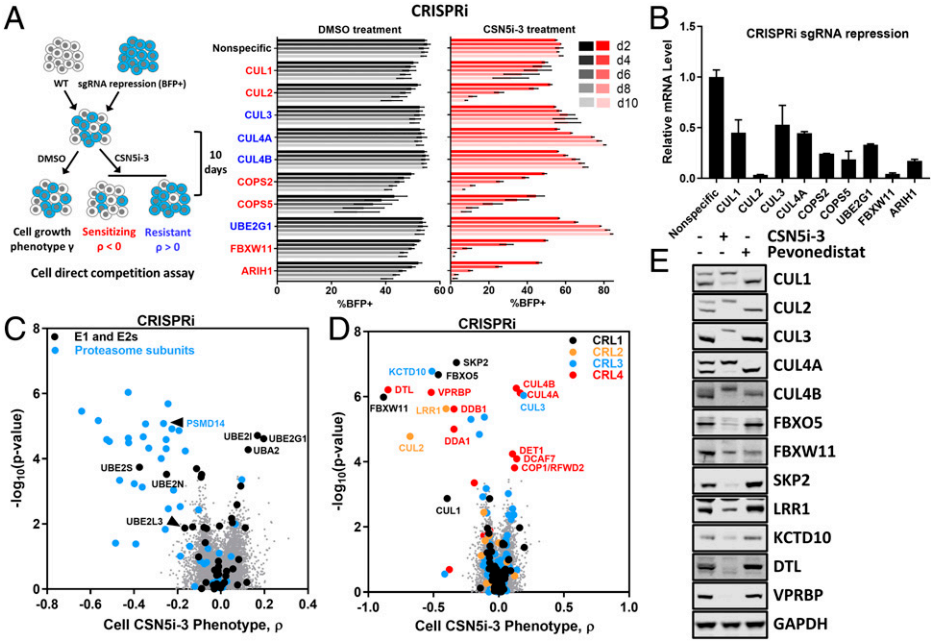

Fig. 3. Genetic validation of screen results by individual sgRNAs. (*A*) CRISPRi screen phenotypes are reproduced by sgRNAs targeting individual genes. K562 cells were infected with individual sgRNAs (BFP$^+$) targeting the indicated genes (two top-scoring sgRNAs in the original screen for each gene; *SI Appendix*, Table S3) and mixed at a 1:1 ratio with parental K562 cells. The cell mixtures were treated with DMSO or 1 μM CSN5i-3, grown for 10 d, and %BFP$^+$ cells was quantified every other day by flow cytometry. Genes whose repression exacerbated or suppressed CSN5i-3 sensitivity in the original screen are color coded red or blue, respectively. Error bars represent ±SD; $n = 2$ technical replicates for each sgRNA. Results of the two sgRNAs for each gene were averaged. (*B*) Extent of gene repression elicited by individual sgRNAs vary. CRISPRi efficiency was evaluated by qRT-PCR, and the relative mRNA levels are shown. The same sgRNAs as in *A* were used. The direct competition assay results observed in *A* could be affected by the differences in CRISPRi efficiency of the individual genes. Error bars represent ±SD; $n = 4$ technical replicates for each sgRNA. Results of the two sgRNAs for each gene were averaged. (*C*) E1, E2, and proteasome gene CRISPRi constructs have divergent effects on CSN5i-3 sensitivity. Volcano plots of CRISPRi phenotype of different sets of genes are highlighted; $n = 2$. (*D*) SgRNA repression of CRL substrate receptor genes have varied effects on CSN5i-3 sensitivity. Substrate receptors are colored black, orange, blue, and red for CRL1, CRL2, CRL3, and CRL4, respectively; $n = 2$. (*E*) Immunoblot confirmation of CRL substrate receptor depletion upon CSN5i-3 treatment of K562 cells. Representative Western blots are shown; $n \geq 2$.

however, uncovered complexity that defied simple explanation. CRISPRi of multiple cullins, SRs, and CRL cofactors rendered cells more sensitive to CSN5i-3, but surprisingly CRISPRa of a subset of these—*CUL1*, *CUL2*, *FBXW11/β-TrCP2*, and *ARIH1*—was also sensitizing (Fig. 2*C*). In contrast to *FBXW11*, the other SRs identified in the CRISPR screens behaved in a more straightforward manner; repression of SRs resulted in heightened sensitivity to CSN5i-3. In particular six SRs in addition to *FBXW11*—*SKP2*, *FBXO5*, *LRR1*, *KCTD10*, *DTL/CDT2*, and *VPRBP*—showed strong sensitivity to CSN5i-3 in the original CRISPRi screen and when individually targeted (Fig. 3 *A* and *D* and *SI Appendix*, Fig. S4*A*). Western blotting of cells confirmed depletion of all these SRs by CSN5i-3 (Fig. 3*E*), consistent with the MS2 data (*SI Appendix*, Fig. S4*F* and Dataset S1). We hypothesize that a significant portion of CSN5i-3's antiproliferative effect was mediated by loss of function of one or more of the corresponding CRLs and accumulation of their cognate substrates (*SI Appendix*, Fig. S4*F*). However, unlike these seven, CRISPRi of *DET1*, *DCAF7*, and *COP1* (CRL4 SRs) rendered cells moderately resistant to CSN5i-3 (Fig. 3*D*). Notably, MS2 results showed an increase in DCAF7 upon CSN5i-3 treatment (DET1 and COP1 were not quantified; Dataset S1), suggesting that these SRs are resistant to autoubiquitylation-induced degradation (AID) and their cognate CRL4 complexes became constitutively active and thereby exerted antiproliferative effects upon CSN inhibition. Consistent with this possibility, CRISPRa of *CUL4A*, *CUL4B*, and the CUL4 E2 enzyme partner *UBE2G1* induced sensitivity to CSN5i-3, whereas CRISPRi evoked resistance, suggesting that unrestrained activity of some CRL4s rendered cells sensitive to CSN inhibition. However, CRISPRi of other CRL4 SRs (*DTL* and *VPRBP*) rendered cells sensitive to CSN5i-3.

Taken together, the CRISPRi and CRISPRa screens suggested two main conclusions. First, CSN5i-3 has very specific effects in that the top hits from both screens are strongly enriched for components, cofactors, or regulators of CRL complexes. Second, the patterns of resistance and sensitivity to CSN5i-3 point to CSN exerting a complex effect on CRL activity. In many cases loss of CSN activity is consistent with reduced abundance for particular CRLs rendering cells sensitive to their further depletion. Conversely, a handful of CRLs appear to be constitutively (hyper)active such that their induction sensitizes cells to CSN5i-3 and their depletion renders them more resistant. These divergent observations can be rationalized based on intrinsic differences in rates of AID between different SRs. We suggest that if an SR is particularly susceptible to AID, it is depleted upon loss of CSN activity and its further repression by CRISPRi renders cells more sensitive to CSN5i-3. Conversely, if it is refractory to AID, it persists in an assembled state in the absence of CSN activity and thereby either sequesters limiting components (e.g., its cullin partner or CSN) or inappropriately degrades neosubstrates, such that its depletion renders cells more tolerant of CSN5i-3.

CSN Inhibition Results in G2 Arrest, DNA Rereplication, and Cell Apoptosis. We next sought to explore more deeply the results of the CRISPR screens to understand the mechanisms by which CSN5i-3 inhibits cell proliferation. We first performed a cell cycle analysis because cell cycle and DNA replication genes were enriched near the top of our hit lists (Fig. 2*D*). K562 cells were treated with 1 μM CSN5i-3 (Fig. 1*C*), and cell cycle distribution was monitored by flow cytometry. As expected, disruption of NEDD8 removal adversely affected cell cycle progression

(45, 48). At 24 h of CSN5i-3 treatment, K562 cells began to accumulate in G2/M phase. By 72 h, a significant fraction of cells contained >4N DNA. Phosphohistone H3 (pHH3) staining indicated that the fraction of cells in mitosis remained unchanged at ∼2% (Fig. 4*A*). G2/M accumulation and DNA overreplication were also observed in other cancer cell lines treated with CSN5i-3 (*SI Appendix*, Fig. S5*A*).

The effect of CSN5i-3 on the cell cycle is reminiscent of cells undergoing DNA rereplication, during which replication origins are fired more than once per cell cycle. Several genetic defects trigger rereplication, including aberrant overexpression of the replication initiation factors CDT1 and CDC6 or depletion of the CDT1 inhibitor GMNN (51–53). Strikingly, *GMNN* was the top hit in the CSN5i-3 CRISPRi screen (Fig. 2*D*) and one of the most sensitive hits in the pevonedistat CRISPRi screen (*SI Appendix*, Fig. S3 *C* and *F*).

GMNN Is a Critical CSN5i-3 Target That Contributes to Effects on the Cell Cycle and Apoptosis. To pursue GMNN, we first reproduced the CRISPRi screen results in a direct competition assay using K562 cell lines stably transduced with constructs that expressed individual control or *GMNN*-directed sgRNA. This confirmed that *GMNN* repression sensitized cells to CSN5i-3 (Fig. 4*B*). A cycloheximide (CHX) chase experiment showed that CSN5i-3 treatment decreased the half-life of GMNN from 8.2 h to 3 h (Fig. 4*C*). CSN5i-3 also caused a time-dependent decrease in GMNN in the absence of CHX in K562 and multiple other cell lines (Fig. 4*D* and *SI Appendix*, Fig. S5B). To evaluate further the connection between GMNN and CSN5i-3 we measured cell cycle profiles and apoptosis in K562 cells depleted of or overexpressing GMNN (Fig. 4 *E* and *F*). Strikingly, CRISPRi of *GMNN* increased apoptosis, G2/M accumulation, and DNA overreplication in response to CSN5i-3, whereas overexpression had the opposite effects. Similar cell cycle responses to *GMNN* knockdown by siRNA were observed in human osteosarcoma U2OS, which has an intact DNA damage response and in colorectal carcinoma HCT116 cells, which are highly sensitive to CSN5i-3 (27) (Fig. 4*G*). These results suggest that GMNN destabilization was a key node that underlies the cellular response to CSN5i-3. Consistent with this hypothesis, repression of multiple DNA licensing factors conferred resistance to CSN5i-3 treatment in the CRISPRi screen (*SI Appendix*, Fig. S5*C*).

GMNN Down-Regulation upon CSN5i-3 Treatment Is Triggered by FBXO5 Degradation. To understand how CSN5i-3 causes GMNN depletion, we investigated proteins that mediate GMNN degradation. GMNN is a substrate of ubiquitin ligase APC/C^{CDH1} (31). The APC/C^{CDH1}-interacting protein and SCF substrate receptor FBXO5/EMI1 showed strong sensitivity to CSN5i-3 in the CRISPRi screen (Fig. 3*D*). FBXO5 directly binds and inhibits APC/C^{CDH1} throughout interphase (54), thereby stabilizing APC/C^{CDH1} substrates like GMNN and cyclin A. Four observations point to CSN5i-3–mediated degradation of FBXO5 as playing a key role in GMNN depletion and DNA rereplication. First, CSN5i-3 reduced the half-life of FBXO5 by threefold in K562 cells (Fig. 4*C*) and had similar effects in multiple other cell lines (*SI Appendix*, Fig. S5*B*). Second, a direct competition growth assay showed that *FBXO5* CRISPRi sensitized cells to CSN5i-3 (Fig. 4*B*), very similar to what was observed for *GMNN*. Third, FBXO5 depletion and overexpression mirrored the effects of GMNN manipulations on cell cycle profile, DNA overreplication, and apoptosis of K562 cells (Fig. 4 *E* and *F*). As was observed for *GMNN*, siRNA directed against *FBXO5* had similar effects in U2OS and HCT116 cell lines (Fig. 4*G*). Fourth, and most important, *FBXO5* CRISPRi enhanced depletion of GMNN in response to CSN5i-3 treatment, whereas *FBXO5* overexpression had the opposite effect and stabilized GMNN (Fig. 4*D*).

To evaluate whether enhanced degradation of FBXO5 in response to CSN5i-3 is due to autoubiquitylation or $SCF^{\beta\text{-}TrCP}$, which mediates turnover of FBXO5 in early mitosis (55, 56), we tested the effect of mutations in FBXO5's phosphodegron that block its binding to β-TrCP. These mutations did not impede CSN5i-3–dependent degradation of FBXO5 (Fig. 4*H*). FBXO5 assembles with CUL1•SKP1 to form a canonical SCF/CRL1 ubiquitin ligase complex (37, 57), and we suggest that failure to deneddylate and disassemble SCF^{FBXO5} complexes resulted in autoubiquitylation and degradation of FBXO5.

In summary, we propose that CSN5i-3 induces FBXO5 autodegradation, resulting in activation of APC/C^{CDH1} during interphase and subsequent premature degradation of its substrates, including GMNN and CCNA2. Ultimately, this leads to G2 delay, DNA rereplication, and apoptosis (Fig. 4*I*).

The CUL4–DTL–SETD8 Pathway Contributes to CSN5i-3 Toxicity. Given the hundreds of CRL complexes, it is likely that disruptions of multiple pathways contribute incrementally to the cytotoxicity induced by CSN inhibition. To identify additional contributory pathways, we examined genes that yielded opposite phenotypes in the CRISPRi and CRISPRa screens. Using cutoff values of $P < 0.05$ and $|\rho| > 0.15$, we identified 56 genes that scored in both CRISPRi and CRISPRa, including *CUL4A* and its SR *DTL* (*SI Appendix*, Table S1). Moreover, *DTL* repression and induction elicited opposing effects on the cell cycle (G2 arrest and DNA rereplication) and apoptosis (Fig. 5 *A* and *B* and *SI Appendix*, Fig. S6 *A* and *B*). CSN inhibition led to loss of DTL protein (Fig. 3*E*), consistent with CRISPRi of *DTL* conferring enhanced sensitivity to CSN5i-3.

$CRL4^{DTL}$ has multiple substrates, including CDT1, CDKN1A/p21, FBH1, SETD8/KMT5a, and SDE2, any of which could account for how it modulates sensitivity to CSN5i-3. Of these, only *SETD8*, a histone H4 lysine 20 methyltransferase, was identified as a hit in either CRISPR screen, and strikingly it showed opposite phenotypes to *DTL* in both screens, identifying it as the most likely candidate to account for the CRISPR phenotypes of *DTL* (*SI Appendix*, Table S1). Consistent with the decrease in DTL levels, SETD8 increased in K562 cells upon CSN5i-3 treatment (*SI Appendix*, Fig. S6*C*), and CHX chase assay showed that it was stabilized by CSN5i-3 (Fig. 5*C*). Because SETD8 oscillates during the cell cycle, peaking at G2/M phase to facilitate chromatin packing (58), we sought to address whether SETD8 stabilization was caused by CSN5i-3–induced G2 arrest. K562 cells were synchronized in early G1/S phase using double thymidine block or in M phase with thymidine followed by nocodazole treatment, and subsequently released into medium containing CSN5i-3 or DMSO. CSN5i-3–treated cells did not show any differences in cell cycle distribution compared to the control in the first 8 h, yet SETD8 levels were increased as early as 2 h following release into CSN5i-3 (Fig. 5*D* and *SI Appendix*, Fig. S6*C*). Moreover, methylated lysine 20 of histone H4 (H4K20Me1), which is a functional readout of SETD8 activity, was also increased with similar kinetics (Fig. 5*D*).

Direct competition assays with *SETD8* CRISPRi and overexpression cells pitted against wild-type cells replicated the results observed in the CRISPR screens, with *SETD8* repression and overexpression enhancing resistance and sensitivity to CSN5i-3 treatment, respectively (Fig. 5*E*). Moreover, the CRISPRi cells also exhibited reduced DNA rereplication and apoptosis by

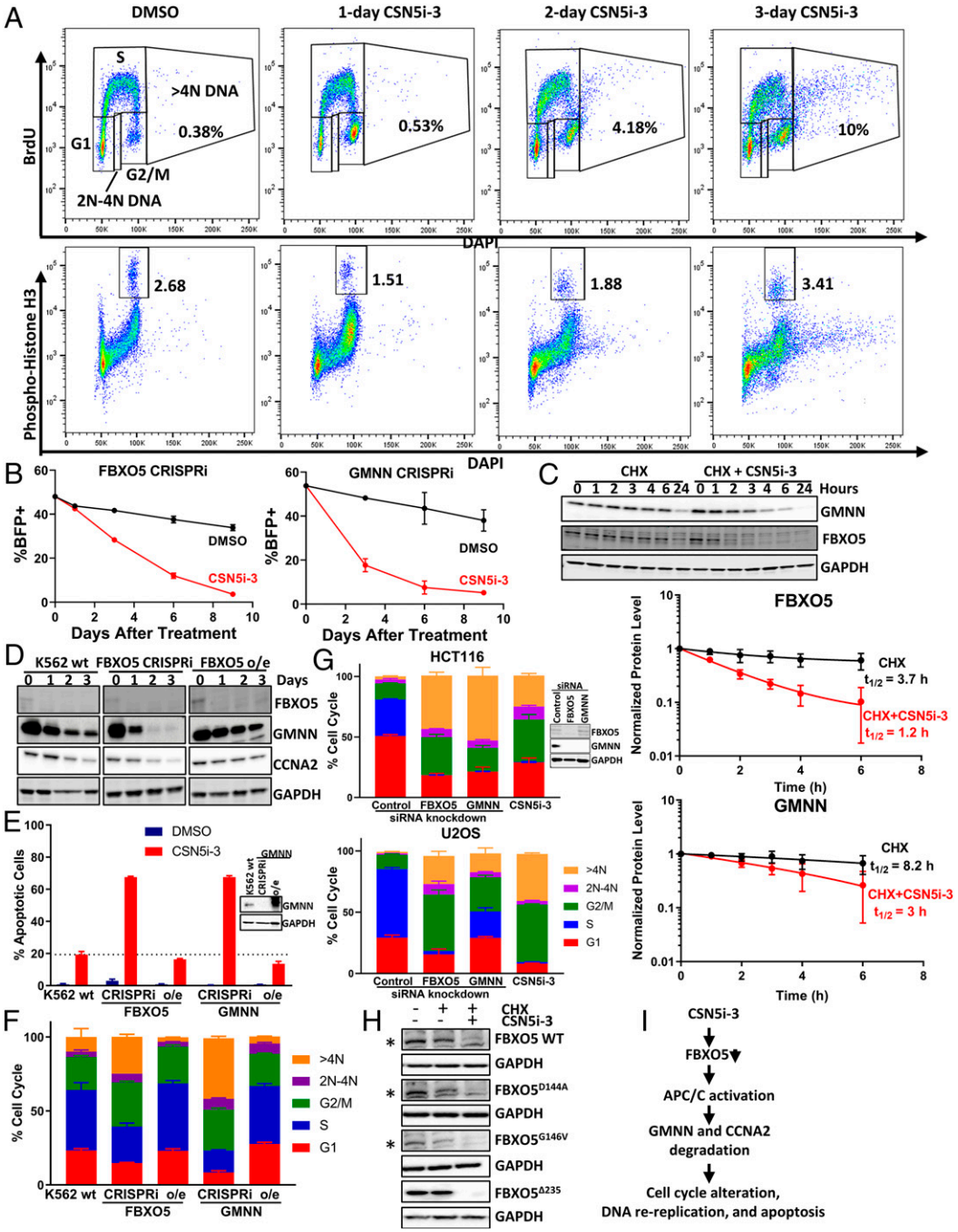

Fig. 4. The SCF^{FBXO5}–APC/C–GMNN pathway is a key mediator of CSN5i-3 toxicity. (*A*) CSN5i-3 induces overreplication of DNA. K562 cells treated with DMSO or 1 μM CSN5i-3 for 1 to 3 d were pulse labeled with bromodeoxyuridine (BrdU), fixed, stained with anti-BrdU and DAPI, and analyzed for cell cycle distribution by flow cytometry (*Upper*). (*Lower*) Same as *Upper* except that cells were stained with fluorescent antibodies to phosphohistone H3 (pHH3) to label cells in mitosis, prior to flow cytometry. Representative graphs are shown; $n \geq 3$. (*B*) Repression of *FBXO5* or *GMNN* sensitizes cells to CSN5i-3. This is the same as in Fig. 3*A* except that sgRNAs (BFP^{+}; the top-scoring one in the original screen; see *SI Appendix*, Table S3) targeting *FBXO5* or *GMNN* were used. Error bars represent ±SD; $n = 2$ to 3. (*C*) CSN5i-3 induces degradation of FBXO5 and GMNN. CHX chase was performed for 0 to 24 h on K562 cells treated with and without 1 μM CSN5i-3. Error bars represent ±SD; $n = 3$. (*D*) GMNN depletion by CSN5i-3 is strongly modulated by FBXO5. A total of 1 μM CSN5i-3 was added for 0 to 3 d to unmodified K562 cells (wild type [WT]) or K562 cells in which *FBXO5* was repressed by CRISPRi or overexpressed (o/e; stable integration of cDNA). Representative Western blots are shown; $n \geq 2$. (*E* and *F*) Transgene-driven overexpression and sgRNA-mediated repression of *FBXO5* or *GMNN* have opposite effects on induction of apoptosis and overreplication by CSN5i-3 in K562 cells. Cells were treated with DMSO or 1 μM CSN5i-3 for 3 d. Apoptosis (*E*) was estimated by measurement of activated Caspase 3. Cell cycle stage/DNA content (*F*) was evaluated as in *A*. GMNN protein levels in untransfected wild-type, repressed, and overexpressed cells are shown by Western blot. Error bars represent ±SD; $n = 3$. (*G*) *FBXO5* knockdown, *GMNN* knockdown, and CSN5i-3 treatment have similar effects on cell cycle profile and overreplication. Cells were treated with siRNA against either *GMNN* or *FBXO5* or with 1 μM CSN5i-3 and incubated for 3 d. Cell cycle stage and DNA content were evaluated as in *A*. FBXO5 and GMNN protein levels in HCT116 cells treated with indicated siRNAs are shown by Western blot. $n = 3$. (*H*) Depletion of FBXO5 by CSN5i-3 is not dependent on the SCF$^{β\text{-}TrCP}$ pathway. K562 cells were stably transfected with constructs that express wild-type FBXO5 or the indicated mutants. All three mutants shown lack the phosphodegron bound by SCF$^{β\text{-}TrCP}$. Transfected cells were treated with DMSO, 50 μg/mL CHX, or CHX plus 1 μM CSN5i-3 for 4 h before immunoblotting. The asterisk denotes the target bands, and the fast-migrating bands below these bands are nonspecific. Representative Western blots are shown; $n = 3$. (*I*) Proposed mechanism of CSN5i-3 toxicity through the SCF^{FBXO5}–APC/C–GMNN axis.

flow cytometry (Fig. 5 *A* and *B* and *SI Appendix*, Fig. S6*A*). These results were also confirmed by shRNA-mediated *SETD8* knockdown (*SI Appendix*, Fig. S6 *D–F*). Overexpression of SETD8, however, elicited no obvious differences in DNA rereplication and apoptosis relative to wild-type cells upon CSN5i-3 treatment (Fig. 5 *A* and *B* and *SI Appendix*, Fig. S6*A*). Lastly, when we performed direct competition growth assays pitting *DTL* and *SETD8* doubly repressed cells against cells in which one or the other gene was repressed, we found that additional depletion of *SETD8* in *DTL* CRISPRi cells was protective (Fig. 5*F*), whereas additional repression of *DTL* in the face of *SETD8* CRISPRi was sensitizing (Fig. 5*G*). Together these findings suggest that other substrates downstream of DTL in addition to SETD8 contribute to sensitivity to CSN5i-3 and that accumulation of SETD8 is necessary but not sufficient to promote rereplication and apoptosis (Fig. 5*H*).

SCF^{FBXO5}–APC/C–GMNN and $CRL4^{DTL}$–SETD8 Pathways Function through CDT1. Given the dramatic and consistent effects of CSN5i-3 on GMNN, FBXO5, DTL, and SKP2 protein levels and the functional relevance of these genes for CSN5i-3 toxicity, the downstream replication initiation factor and GMNN target, CDT1, was investigated further. CDT1 protein levels were minimally affected in K562 as well as other cell lines upon CSN5i-3 treatment (*SI Appendix*, Fig. S5*B*). *CDT1* repression resulted in a mild increase in sensitivity to CSN5i-3, whereas it conferred resistance to pevonedistat treatment (*SI Appendix*, Fig. S7*A*), consistent with prior reports (28, 29). In double depletion experiments, additional CRISPRi of *CDT1* in cells in which *DTL*, *FBXO5*, or *GMNN* was repressed rendered cells more resistant to CSN5i-3 treatment than the singly perturbed cells (Fig. 6*A*). Together these data suggest that the contributions of these factors to CSN5i-3 toxicity converge on CDT1 and replication licensing.

To evaluate the impact of other SRs on CSN5i-3 cytotoxicity, we examined cell cycle parameters and apoptosis upon CRISPRi repression and ectopic overexpression of the seven SRs identified in the CRISPRi screen. Modulation of *DTL* had the strongest effects, followed by *FBXO5* and *SKP2* (*SI Appendix*, Fig. S7 *B* and *C*). Considering that SKP2 and DTL promote degradation of overlapping substrates, including CDT1, we suggest that the SKP2 pathway also converges on replication licensing.

CSN Inhibition Induces DNA Damage Response Consistent with Rereplication. CDT1 overexpression or GMNN ablation induces DNA rereplication (51–53). Rereplication is known to induce single-strand DNA breaks and elicit DNA damage signaling, which eventually lead to apoptosis. Given the impact of CSN5i-3 on rereplication control, we monitored its effect on signaling pathways activated by single- and double-strand DNA breaks.

Inhibiting CSN function in K562 and HCT116 cells activated a DNA damage checkpoint response marked by accumulation of pCHK1 (pSer317), pRAD17 (pSer645), pCHK2 (pThr68), and γH2AX (pSer139) (Fig. 6*B*). Surprisingly, total CHK1 and CHK2 levels were decreased upon CSN5i-3 treatment in a subset of cell lines; previous reports showed that CHK1 and CHK2 are CRL substrates (59–61), and thus may be subject to CSN5i-3 regulation. Accumulation of pCHK1 and pRAD17 is consistent with activation of ATR and recruitment of the RAD17•RFC and 9•1•1 repair complexes to sites of single-strand DNA damage. Notably, the CRISPRi screen identified multiple players in the ATR pathway whose repression caused heightened sensitivity to CSN5i-3 (*SI Appendix*, Fig. S7*D*), suggesting that ATR signaling protects cells from CSN5i-3. In light of this result, we evaluated the specific ATR inhibitor, BAY-1895344, for synergy with CSN5i-3. We observed strong synergy in K562 and HCT116 cell lines regardless of p53 status (Fig. 6*C* and *SI Appendix*, Fig. S7*E*). ATM target pCHK2 and the double-strand DNA damage marker γH2AX were also increased in K562 cells treated with CSN5i-3, as well as in other cancer cell lines (Fig. 6*B* and *SI Appendix*, Fig. S7*F*).

Notably, the CRISPRi screen identified components of the ATR pathway but not the ATM pathway (Dataset S3). This is likely because p53 is mutated in K562 cells, and p53 is a major downstream effector protein of ATM signaling (62, 63). In contrast, HCT116 is wild type for p53, and DNA rereplication and apoptosis were observed with more rapid kinetics after CSN5i-3 treatment (*SI Appendix*, Fig. S7*G*). To test whether p53 may play a role in mediating ATM dependence in cells exposed to CSN5i-3, we tested the ATM inhibitor KU-60019 in isogenic *TP53* wild-type and null HCT116 cell lines and found that CSN5i-3 and KU-60019 displayed enhanced synergy in the wild-type p53 background (Fig. 6*D*). Further study showed that p53 was not required for but enhanced apoptosis in response to CSN5i-3 (Fig. 6*E*). Conversely, wild-type p53 restrained DNA rereplication (Fig. 6*F*). Previous reports demonstrated that p21 plays a survival role in preventing p53-dependent apoptosis upon DNA damage, particularly in HCT116 cells (64). CSN5i-3 treatment resulted in p21 accumulation in p53 wild-type HCT116 cells, but not in p53 null cells (Fig. 6*G*), which may account for the divergent effects of p53 on induction of apoptosis and rereplication by CSN5i-3.

***GMNN* Dependency and Cancer Sensitivity to CSN5i-3.** To identify cancers that may have increased sensitivity to CSN5i-3 treatment, we searched the Cancer Dependency Map (DepMap) for cancer cells lines that are especially sensitive to *GMNN* knockout by CRISPR (DepMap 21Q2 Public+Score, CERES score for unscaled gene effect). This suggested that nonsmall cell lung cancer (NSCLC) and pancreatic cancer have higher dependency on *GMNN* compared to other cancers. When the extent of DNA rereplication upon CSN5i-3 treatment was plotted against the gene effect of *GMNN* knockout in a number of cell lines, a rough correlation was observed (*SI Appendix*, Fig. S7*H*), suggesting that *GMNN* essentiality might be a useful parameter for predicting sensitivity to CSN5i-3.

Discussion

We previously proposed the adaptive exchange hypothesis (*SI Appendix*, Fig. S1*A*), which posits that the k_{off} of a substrate receptor•adaptor complex from a CRL is modulated by the substrate, NEDD8, and CAND1, and that this determines the cellular repertoire of CRL complexes (32). NEDD8–CRL complexes are very stable due to slow dissociation of the modular SR•adaptor subcomplex from the cullin•RING catalytic core (33). If the substrate is bound to the NEDD8–CRL, this situation pertains. However, once unoccupied, a NEDD8–CRL can rapidly bind CSN, which deconjugates NEDD8 from the cullin subunit, thereby quenching ubiquitin ligase activity. Upon dissociation of CSN, the deactivated CRL complex binds CAND1, which expels the SR•adaptor, clearing the way for a different SR•adaptor to bind. CAND1 also recruits NEDD8-conjugating factors, such that upon its dissociation by an SR•adaptor and exposure of the NEDD8 conjugation site, the newly formed CRL is neddylated to generate an active NEDD8–CRL complex and the cycle begins anew (32). The speed of the exchange cycle coupled with the plasticity that it affords allows a limited number of cullin•RING catalytic cores

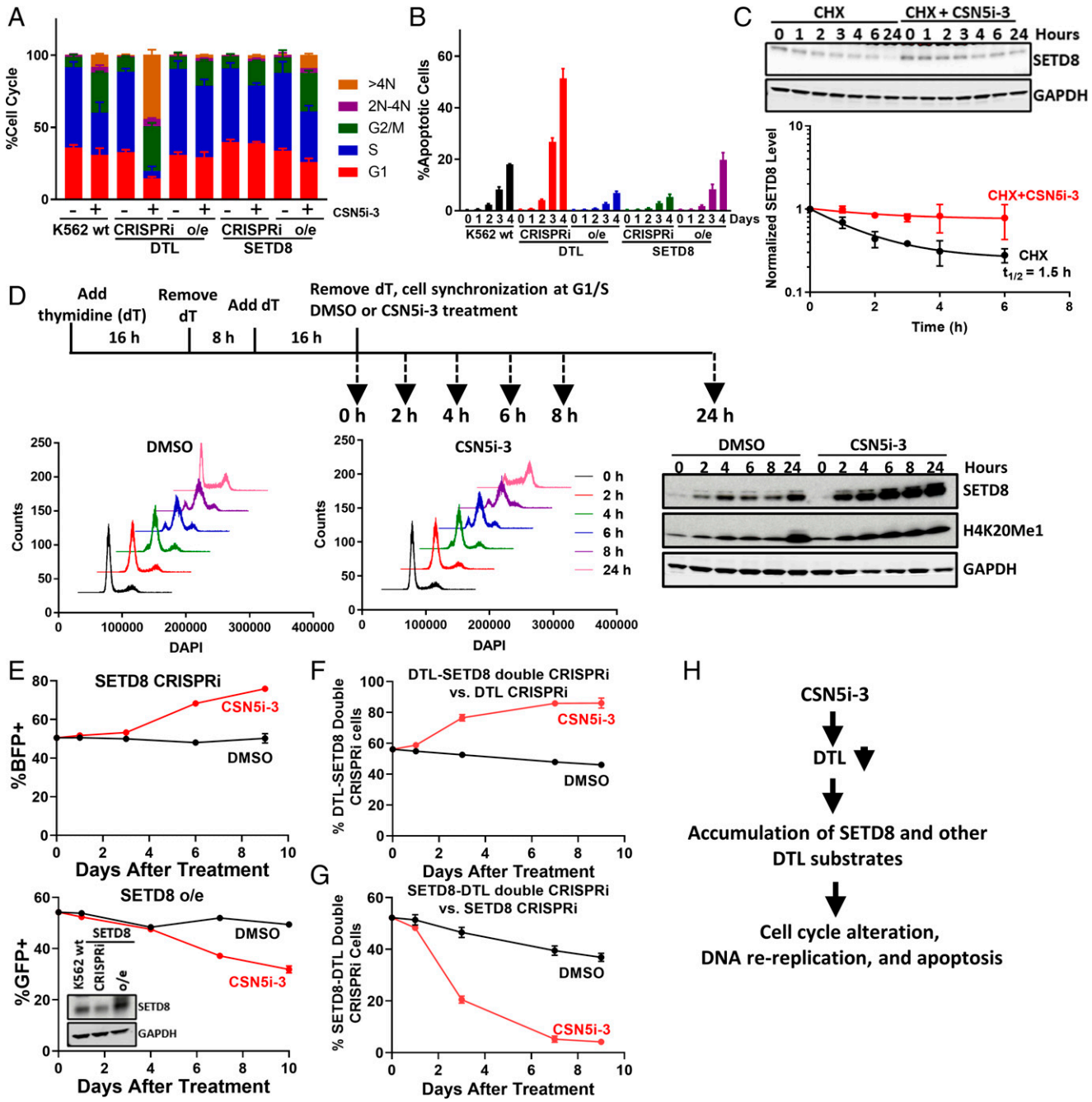

Fig. 5. The CRL4^{DTL}–SETD8 pathway contributes to CSN5i-3 toxicity. (*A* and *B*) Repression and overexpression of *DTL* have opposite effects on induction of overreplication and apoptosis by CSN5i-3. Unmodified K562 cells (WT) or cells in which either *DTL* or *SETD8* was repressed (CRISPRi) or overexpressed (o/e; stable integration of cDNA) were treated for 3 (*A*) or 1 to 4 (*B*) days with DMSO or 1 μM CSN5i-3. Cell cycle stage/DNA content (*A*) and apoptosis (*B*) were evaluated by fluorescence-activated cell sorting (FACS) as in Fig. 4. Error bars represent ±SD; $n = 3$. (*C*) CSN5i-3 blocks SETD8 degradation. CHX chase was performed for 0 to 24 h in K562 cells treated with or without 1 μM CSN5i-3. Error bars represent ±SD; $n = 3$. (*D*) Up-regulation of SETD8 by CSN5i-3 is not an indirect consequence of G2 arrest. K562 cells were synchronized at the G1/S boundary by double thymidine (dT) block and then released in the presence of either DMSO or 1 μM CSN5i-3. At the indicated times, samples were withdrawn, and cells were assessed by FACS to determine cell cycle stage, or cell lysates were prepared and evaluated for content of SETD8 or its reaction product H4K20Me1 by immunoblotting. Representative Western blots are shown; $n = 3$. (*E*) SETD8 modulates cytotoxicity of CSN5i-3. This is the same as in Fig. 3*A* except that K562 cells in which *SETD8* was repressed (CRISPRi; BFP$^+$) or overexpressed (o/e; GFP$^+$) were mixed with parental K562 cells. SETD8 protein levels in wild-type, repressed, and overexpressed cells are shown by Western blot. Error bars represent ±SD; $n = 3$. (*F*) SETD8 contributes to the CSN5i-3 sensitivity of DTL-deficient cells. This is the same as in Fig. 3*A* except that K562 cells with CRISPRi repression of both *DTL* and *SETD8* (GFP$^+$BFP$^+$) were mixed 1:1 at time 0 with cells with CRISPRi for only *DTL* (GFP$^+$). Error bars represent ±SD; $n = 3$. (*G*) DTL deficiency renders cells sensitive to CSN5i-3 by mechanisms in addition to SETD8 accumulation. This is the same as in *F* except that cells with CRISPRi repression of both *DTL* and *SETD8* (GFP$^+$BFP$^+$) were cocultured with CRISPRi for only *SETD8* (GFP$^+$). Error bars represent ±SD; $n = 3$. (*H*) Proposed mechanism of CSN5i-3 toxicity through the CRL4^{DTL}–SETD8 axis.

to form a broad, rapidly evolving array of distinct CRL complexes. This in turn may enable large variations in SR expression during development and in SR gene number during evolution.

In this work, we sought to explore further this hypothesis and its implications. Key to this effort was the availability of a potent and selective CSN inhibitor, which should block the cycle by preventing deconjugation of NEDD8 from CRLs not occupied by the substrate. This halts the exchange process because NEDD8 blocks binding of CAND1 to cullins (33). Prior work has shown that inhibition of CSN by CSN5i-3

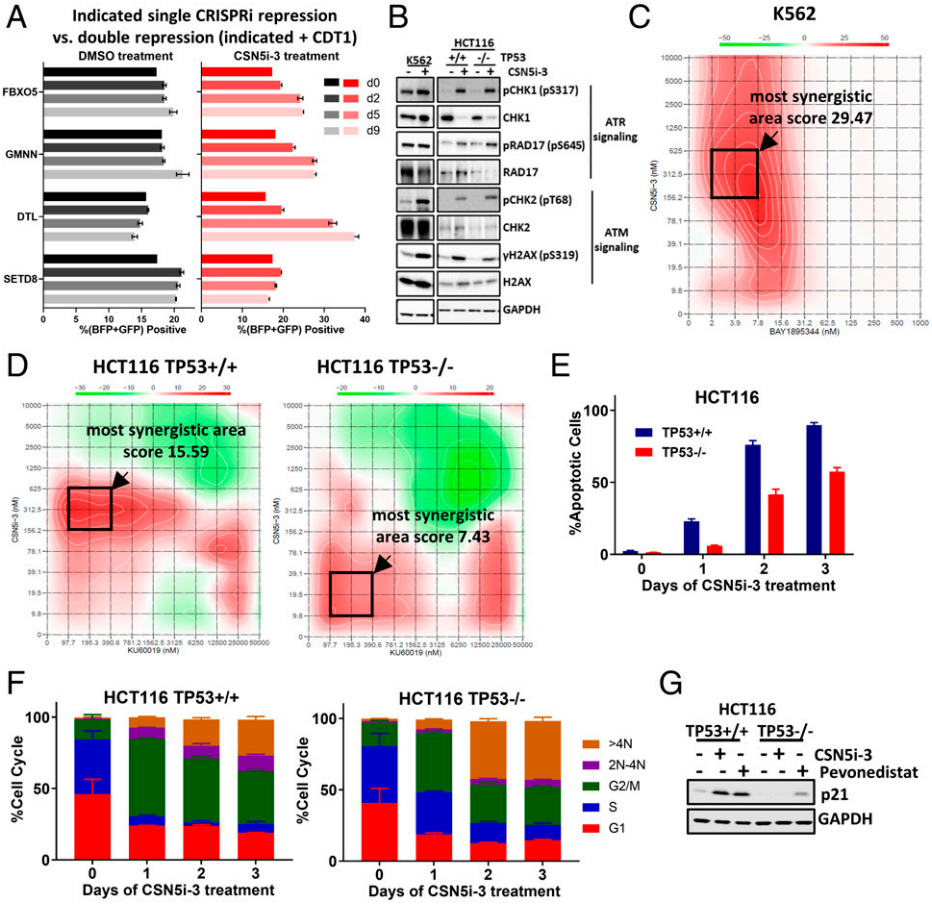

Fig. 6. CSN5i-3 chemical–genetic interactions are reproducible and found in multiple cell lines. (*A*) FBXO5, GMNN, and DTL exert their effects through CDT1. Direct competition assays of the indicated gene plus *CDT1* double CRISPRi (GFP^+BFP^+) cells vs. the indicated single CRISPRi cells (GFP^+) were performed. CSN5i-3 sensitivity conferred by *FBXO5*, *GMNN*, or *DTL* repression (Fig. 4*B* and *SI Appendix*, Fig. S4*A*) was relieved by corepression of *CDT1*. Error bars represent ±SD; $n = 3$. (*B*) CSN5i-3 activates signaling through the ATR and ATM DNA damage response pathways. All cells were treated with 1 μM CSN5i-3 for 3 d. Representative Western blots are shown; $n = 3$. (*C*) CSN5i-3 and the specific ATR inhibitor BAY-1895344 synergistically inhibit cell proliferation. K562 cells were treated with drugs for 3 d, and proliferation was assessed by CellTiter-Glo assay; $n = 4$. Synergy was calculated using SynergyFinder (77) using the ZIP (zero interaction potency) model. The most synergistic area score, which represents the most synergistic 3-by-3 dose window in a dose–response matrix, is shown. Scores larger than 10 are generally considered to be indicative of synergy. (*D*) CSN5i-3 and the ATM inhibitor KU-60019 are synergistic in HCT116 cells with wild-type p53. This is the same as in *C*, except that CSN5i-3 and KU-60019 were evaluated in *TP53* wild-type and null HCT116 cell lines; $n = 2$. (*E*) Apoptosis analysis of *TP53* wild-type and null HCT116 cells. Apoptosis was estimated by measurement of activated Caspase 3. Error bars represent ±SD; $n = 3$. (*F*) Loss of p53 exacerbates DNA overreplication in HCT116 cells. Cell cycle stage/DNA content was evaluated by FACS as in Fig. 4*A*. Error bars represent ±SD; $n = 3$. (*G*) p53 is required for CSN5i-3–mediated induction of p21 in HCT116 cells. Cells were treated with 1 μM CSN5i-3 or pevonedistat for 24 h. Representative Western blots are shown; $n = 3$.

results in depletion of some SRs (27, 38). This is thought to result from autoubiquitylation and subsequent degradation of SRs that are not bound to the substrate but are nevertheless not disassembled from cullin due to blockade of the exchange cycle. Here, we assessed the global impact of CSN inhibition on the proteome from both a physical and functional perspective. Whole proteome mass spectrometry revealed that CSN inhibition caused depletion of multiple CRL pathway components and accumulation of CRL substrates. Meanwhile, CRISPRi and CRISPRa functional screens revealed that cellular sensitivity to CSN5i-3 was profoundly influenced by CRL pathway components. Repression of numerous CRL pathway genes increased sensitivity to CSN5i-3, consistent with the idea that blockade of adaptive exchange results in reduced CRL activity. Conversely, repression of several CRL pathway genes resulted in elevated resistance to CSN5i-3. CSN5i-3 causes accumulation of cullins in an activated, NEDD8-conjugated state. If an SR is susceptible to autoubiquitylation, this can lead to its rapid degradation. However, for NEDD8–CRL^{SR} complexes not prone to autoubiquitylation, the enzyme would be trapped in a permanently activated state in which the bound SR could either block access of other SRs to the cullin or inappropriately ubiquitylate substrates and neosubstates. Alternatively, the intact NEDD8–CRL could serve as a sink by trapping CSN•CSN5i-3 in a ternary complex, resulting in further depletion of cellular CSN activity. In either case, depletion of the SR would be predicted to diminish sensitivity to CSN5i-3. In some cases, induction or repression of a CRL pathway gene increased sensitivity to CSN5i-3. These examples emphasize the delicate balance required to sustain a dynamic network of complexes in which a large excess of SR•adaptors share a limiting number of cullin•RING catalytic cores.

This initial analysis of the CRISPR screen results affirmed the specificity of CSN5i-3 and the importance of adaptive exchange to proper maintenance of functional CRL networks. The CRISPRi screen pointed to effects of CSN inhibition on DNA replication through GMNN down-regulation. GMNN is a negative regulator of DNA replication origin licensing that prevents origins from being fired again in the cell cycle after the initiation of DNA replication (65). Degradation of GMNN via APC/C^{CDH1} during mitosis allows for origin firing in the subsequent cell cycle (31). Normally, APC/C^{CDH1} is shut off upon entry into S phase, which allows GMNN to accumulate (66). APC/C^{CDH1} is maintained in the off state during interphase by FBXO5 (54). CSN5i-3 led to reduced

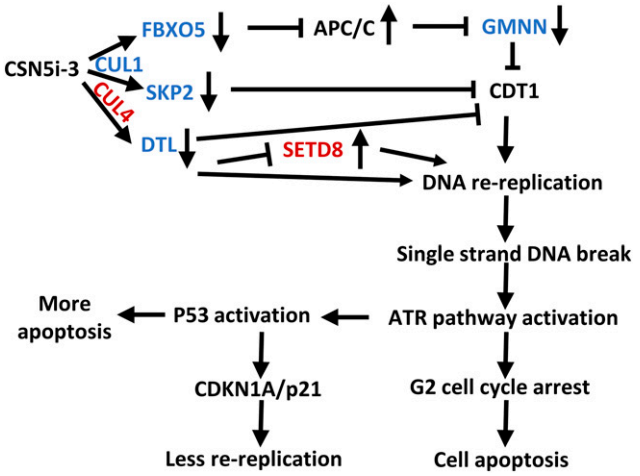

Fig. 7. Proposed model for induction of DNA overreplication and cell apoptosis by CSN5i-3. Upward and downward arrows indicate directional effects of CSN5i-3 on protein levels. Blue and red indicate genes whose CRISPRi-mediated repression renders cells more sensitive and resistant to CSN5i-3, respectively.

levels of FBXO5 due to its increased degradation. This led to unscheduled activation of APC/C^{CDH1} in interphase and premature degradation of GMNN and cyclin A. CDT1 unleashed from GMNN promoted rereplication. Consistent with inappropriate replication being a key mechanism of CSN5i-3 sensitization, repression of multiple components of the ORC and MCM complexes that drive origin firing rendered cells less sensitive to the drug. Other prominent CRISPRi hits are also linked to rereplication control. Both SKP2 and DTL were depleted by CSN5i-3 and their repression by CRISPRi sensitized cells to the drug. These CRL substrate receptors are known to target CDT1 for ubiquitination and degradation (8, 52, 67, 68). The histone H4 lysine 20 methylase SETD8 (69) was also identified as a CRISPRi hit. SETD8 is a substrate of $CRL4^{DTL}$ (70, 71) and repression of SETD8 rendered cells less sensitive to CSN5i-3. SETD8 has also been implicated in control of replication licensing but the exact molecular mechanism remains unknown (72, 73). Further evidence of the intimate connection between CSN function and origin licensing is provided by comparing our results with those from a screen for factors that prevent excess genome replication in HCT116 cells (74). That screen identified 42 genes that were sorted into eight different cell cycle processes, including seven genes related to origin licensing. Our CRISPRi screen identified 22 of the 42 genes as conferring strong sensitization to CSN5i-3, including five of the seven related to origin licensing (*SI Appendix*, Table S2). A model that ties together the screen hits that relate to rereplication control is shown in Fig. 7, with the directional effect of CSN5i-3 on protein levels depicted by upward or downward arrows and the effect of CRISPRi on drug response indicated by font color (sensitive, blue; resistant, red).

A previous study showed that GMNN depletion selectively induced DNA rereplication and apoptosis only in some cancer cells, while combined depletion of GMNN and CCNA2 induces robust DNA rereplication in both cancer and normal cells (53). CSN5i-3 treatment led to FBXO5 depletion, APC/C^{CDH1} activation, and subsequent depletion of APC/C^{CDH1} substrates, including GMNN and CCNA2 (*SI Appendix*, Fig. S5*B*). This may explain why all the tested cancer cell lines in this study, including HeLa, which is insensitive to GMNN depletion (53), showed DNA rereplication and cell apoptosis upon CSN5i-3 treatment.

Our results suggest several approaches for leveraging CSN inhibition for treatment of cancer. Inappropriate reinitiation of DNA replication in G2 upon treatment with CSN5i-3 results in a pattern of DNA damage signaling, characteristic of cells experiencing replication stress, including activation of ATR, CHK1, and RAD17. Notably, CSN5i-3 displayed strong synergy with the ATR inhibitor BAY-1895344. It may be productive to explore the potential to inhibit CSN in combination with drugs that block DNA damage response signaling or in cancers that exhibit activation of and heightened dependence on the ATR pathway.

Materials and Methods

Reagents. CSN5i-3 was generously provided by Novartis. Pevonedistat (MLN4924) was purchased from Active Biochem. BAY-1895344 and KU-60019 were purchased from ApexBio.

Quantitative Proteome Analysis. K562 cells were treated with DMSO or 1 μM CSN5i-3 for 2, 8, and 24 h in four replicates, and cells were harvested and washed once in phosphate buffered saline (PBS) at the indicated time points before cell pellets were snap frozen. The detailed proteomics method is included in *SI Appendix*. The mass spectrometry proteomics data have been deposited to the ProteomeXchange Consortium via the PRIDE partner repository with the dataset identifier PXD027862.

Genome-Wide CRISPRi and CRISPRa Screens. The genome-scale screens were conducted the same way as described previously (40, 75). The hCRISPRi-v2 or hCRISPRa-v2 sgRNA libraries (40) were transduced in duplicate into K562 CRISPRi or CRISPRa cells, respectively. Sequencing analyses were performed as described previously (40, 76). Negative control genes were generated and phenotypes and Mann–Whitney *P* values were calculated as described before. Two phenotype values were calculated for each sgRNA: drug (CSN5i-3 or pevonedistat) sensitivity phenotype (ρ) and cell growth phenotype (γ). Detailed screen method is included in *SI Appendix*.

Quantification and Statistical Analysis. Sequencing counts from CRISPR screens were processed using the Python-based ScreenProcessing pipeline (https://github.com/mhorlbeck/ScreenProcessing) (40). Details of methods to calculate phenotypes and *P* values have been described previously (40, 76). All additional CRISPR screen data analyses were performed in Python 2.7 using a combination of Numpy (v1.12.1), Pandas (v0.17.1), and Scipy (v0.17.0).

Data, Materials, and Software Availability. Mass spectrometry proteomics data have been deposited to the ProteomeXchange Consortium via the PRIDE partner repository (PXD027862) (78). The data will be openly available upon publication.

ACKNOWLEDGMENTS. We thank Novartis for providing the CSN5i-3 compound; Marc Payton and Grace Chung for their help with cell cycle and apoptosis analysis; Sandy Cole for her help with flow cytometry setup and maintenance; Jeanette G. Cook, Julie Bailis, and Paul Hughes for their critical reading and helpful comments of the manuscript; and all members of the R.J.D. laboratory for helpful discussions. Next-generation sequencing was in part performed in the University of California San Francisco Center for Advanced Technology. M.J. was supported by NIH grant K99 GM130964. J.S.W. is a Howard Hughes Medical Institute investigator.

Author affiliations: [a]Oncology Research, Amgen Research, Thousand Oaks, CA 91320; [b]Department of Cellular and Molecular Pharmacology, University of California, San Francisco, CA 94158; [c]California Institute for Quantitative Biosciences, University of California, San Francisco, CA 94158; [d]HHMI, University of California, San Francisco, CA 94158; [e]Genome Analysis Unit, Amgen Research, South San Francisco, CA, 94080; [f]Proteome Exploration Laboratory, Beckman Institute, California Institute of Technology, Pasadena, CA 91125; [g]Amgen Research, Thousand Oaks, CA 91320; and [h]Division of Biology and Biological Engineering, California Institute of Technology, Pasadena, CA 91125

Author contributions: Y.Z., J.R.L., and R.J.D. designed research; Y.Z., M.J., R.A.P., D.L., and J.L. performed research; Y.Z., M.J., R.A.P., D.L., J.L., B.L., S.D.G., C.-M.L., and J.S.W.

contributed new reagents/analytic tools; Y.Z., M.J., D.L., B.L., S.D.G., C.-M.L., and J.S.W. analyzed data; Y.Z. and R.J.D. wrote the paper; and R.J.D. supervised the research.

Competing interest statement: Y.Z. is an employee of Amgen. D.L., C.-M. L., and R.J.D. are employees and shareholders of Amgen. J.L. was an employee of Amgen. J.R.L. was an employee and shareholder of Amgen. M.J. consults for Maze Therapeutics and Gate Biosciences. S.D.G. is the founder, president, CEO, and CTO of Proteas Bioanalytics, Inc. The work described in the paper does not have any direct financial implications for Amgen.

1. T. Cardozo, M. Pagano, The SCF ubiquitin ligase: Insights into a molecular machine. *Nat. Rev. Mol. Cell Biol.* **5**, 739–751 (2004).
2. A. R. Willems, M. Schwab, M. Tyers, A hitchhiker's guide to the cullin ubiquitin ligases: SCF and its kin. *Biochim. Biophys. Acta* **1695**, 133–170 (2004).
3. R. J. Deshaies, C. A. Joazeiro, RING domain E3 ubiquitin ligases. *Annu. Rev. Biochem.* **78**, 399–434 (2009).
4. T. A. Soucy *et al.*, An inhibitor of NEDD8-activating enzyme as a new approach to treat cancer. *Nature* **458**, 732–736 (2009).
5. R. I. Enchev, B. A. Schulman, M. Peter, Protein neddylation: Beyond cullin-RING ligases. *Nat. Rev. Mol. Cell Biol.* **16**, 30–44 (2015).
6. K. Baek *et al.*, NEDD8 nucleates a multivalent cullin-RING-UBE2D ubiquitin ligation assembly. *Nature* **578**, 461–466 (2020).
7. D. C. Scott *et al.*, Two distinct types of E3 ligases work in unison to regulate substrate ubiquitylation. *Cell* **166**, 1198–1214.e24 (2016).
8. D. Horn-Ghetko *et al.*, Ubiquitin ligation to F-box protein targets by SCF-RBR E3-E3 super-assembly. *Nature* **590**, 671–676 (2021).
9. K. Baek, D. C. Scott, B. A. Schulman, NEDD8 and ubiquitin ligation by cullin-RING E3 ligases. *Curr. Opin. Struct. Biol.* **67**, 101–109 (2021).
10. S. Hill *et al.*, Robust cullin-RING ligase function is established by a multiplicity of poly-ubiquitylation pathways. *eLife* **8**, e51163 (2019).
11. Q. L. Sievers, J. A. Gasser, G. S. Cowley, E. S. Fischer, B. L. Ebert, Genome-wide screen identifies cullin-RING ligase machinery required for lenalidomide-dependent CRL4^{CRBN} activity. *Blood* **132**, 1293–1303 (2018).
12. D. M. Duda *et al.*, Structure of HHARI, a RING-IBR-RING ubiquitin ligase: Autoinhibition of an ariadne-family E3 and insights into ligation mechanism. *Structure* **21**, 1030–1041 (2013).
13. K. Wu, J. Kovacev, Z. Q. Pan, Priming and extending: A UbcH5/Cdc34 E2 handoff mechanism for polyubiquitination on a SCF substrate. *Mol. Cell* **37**, 784–796 (2010).
14. T. Kurz *et al.*, The conserved protein DCN-1/Dcn1p is required for cullin neddylation in C. elegans and S. cerevisiae. *Nature* **435**, 1257–1261 (2005).
15. D. Liakopoulos, G. Doenges, K. Matuschewski, S. Jentsch, A novel protein modification pathway related to the ubiquitin system. *EMBO J.* **17**, 2208–2214 (1998).
16. F. Osaka *et al.*, A new NEDD8-ligating system for cullin-4A. *Genes Dev.* **12**, 2263–2268 (1998).
17. L. Gong, E. T. H. Yeh, Identification of the activating and conjugating enzymes of the NEDD8 conjugation pathway. *J. Biol. Chem.* **274**, 12036–12042 (1999).
18. D. T. Huang *et al.*, E2-RING expansion of the NEDD8 cascade confers specificity to cullin modification. *Mol. Cell* **33**, 483–495 (2009).
19. S. Lyapina *et al.*, Promotion of NEDD-CUL1 conjugate cleavage by COP9 signalosome. *Science* **292**, 1382–1385 (2001).
20. G. A. Cope *et al.*, Role of predicted metalloprotease motif of Jab1/Csn5 in cleavage of Nedd8 from Cul1. *Science* **298**, 608–611 (2002).
21. N. Wei, X. W. Deng, Making sense of the COP9 signalosome. A regulatory protein complex conserved from Arabidopsis to human. *Trends Genet.* **15**, 98–103 (1999).
22. S. Rozen *et al.*, CSNAP is a stoichiometric subunit of the COP9 signalosome. *Cell Rep.* **13**, 585–598 (2015).
23. G. A. Cope, R. J. Deshaies, COP9 signalosome: A multifunctional regulator of SCF and other cullin-based ubiquitin ligases. *Cell* **114**, 663–671 (2003).
24. S. Wee, R. K. Geyer, T. Toda, D. A. Wolf, CSN facilitates cullin-RING ubiquitin ligase function by counteracting autocatalytic adapter instability. *Nat. Cell Biol.* **7**, 387–391 (2005).
25. G. A. Cope, R. J. Deshaies, Targeted silencing of Jab1/Csn5 in human cells downregulates SCF activity through reduction of F-box protein levels. *BMC Biochem.* **7**, 1 (2006).
26. M. H. Lee, R. Zhao, L. Phan, S. C. Yeung, Roles of COP9 signalosome in cancer. *Cell Cycle* **10**, 3057–3066 (2011).
27. A. Schlierf *et al.*, Targeted inhibition of the COP9 signalosome for treatment of cancer. *Nat. Commun.* **7**, 13166 (2016).
28. M. A. Milhollen *et al.*, Inhibition of NEDD8-activating enzyme induces rereplication and apoptosis in human tumor cells consistent with deregulating CDT1 turnover. *Cancer Res.* **71**, 3042–3051 (2011).
29. J. J. Lin, M. A. Milhollen, P. G. Smith, U. Narayanan, A. Dutta, NEDD8-targeting drug MLN4924 elicits DNA rereplication by stabilizing Cdt1 in S phase, triggering checkpoint activation, apoptosis, and senescence in cancer cells. *Cancer Res.* **70**, 10310–10320 (2010).
30. S. P. Bell, A. Dutta, DNA replication in eukaryotic cells. *Annu. Rev. Biochem.* **71**, 333–374 (2002).
31. T. J. McGarry, M. W. Kirschner, Geminin, an inhibitor of DNA replication, is degraded during mitosis. *Cell* **93**, 1043–1053 (1998).
32. X. Liu *et al.*, Cand1-mediated adaptive exchange mechanism enables variation in F-box protein expression. *Mol. Cell* **69**, 773–786.e6 (2018).
33. N. W. Pierce *et al.*, Cand1 promotes assembly of new SCF complexes through dynamic exchange of F box proteins. *Cell* **153**, 206–215 (2013).
34. E. S. Fischer *et al.*, The molecular basis of CRL4DDB2/CSA ubiquitin ligase architecture, targeting, and activation. *Cell* **147**, 1024–1039 (2011).
35. R. I. Enchev *et al.*, Structural basis for a reciprocal regulation between SCF and CSN. *Cell Rep.* **2**, 616–627 (2012).
36. E. D. Emberley, R. Mosadeghi, R. J. Deshaies, Deconjugation of Nedd8 from Cul1 is directly regulated by Skp1-F-box and substrate, and the COP9 signalosome inhibits deneddylated SCF by a noncatalytic mechanism. *J. Biol. Chem.* **287**, 29679–29689 (2012).
37. J. M. Reitsma *et al.*, Composition and regulation of the cellular repertoire of SCF ubiquitin ligases. *Cell* **171**, 1326–1339.e14 (2017).
38. C. Mayor-Ruiz *et al.*, Plasticity of the cullin-RING ligase repertoire shapes sensitivity to ligand-induced protein degradation. *Mol. Cell* **75**, 849–858.e8 (2019).
39. K. M. Reichermeier *et al.*, PIKES analysis reveals response to degraders and key regulatory mechanisms of the CRL4 network. *Mol. Cell* **77**, 1092–1106.e9 (2020).
40. M. A. Horlbeck *et al.*, Compact and highly active next-generation libraries for CRISPR-mediated gene repression and activation. *eLife* **5**, e19760 (2016).
41. L. A. Gilbert *et al.*, CRISPR-mediated modular RNA-guided regulation of transcription in eukaryotes. *Cell* **154**, 442–451 (2013).
42. M. E. Tanenbaum, L. A. Gilbert, L. S. Qi, J. S. Weissman, R. D. Vale, A protein-tagging system for signal amplification in gene expression and fluorescence imaging. *Cell* **159**, 635–646 (2014).
43. M. Kampmann, M. C. Bassik, J. S. Weissman, Integrated platform for genome-wide screening and construction of high-density genetic interaction maps in mammalian cells. *Proc. Natl. Acad. Sci. U.S.A.* **110**, E2317–E2326 (2013).
44. S. T. Nawrocki, P. Griffin, K. R. Kelly, J. S. Carew, MLN4924: A novel first-in-class inhibitor of NEDD8-activating enzyme for cancer therapy. *Expert Opin. Investig. Drugs* **21**, 1563–1573 (2012).
45. J. L. Blank *et al.*, Novel DNA damage checkpoints mediating cell death induced by the NEDD8-activating enzyme inhibitor MLN4924. *Cancer Res.* **73**, 225–234 (2013).
46. H. Mao, Y. Sun, Neddylation-independent activities of MLN4924. *Adv. Exp. Med. Biol.* **1217**, 363–372 (2020).
47. L. Zhou, L. Jia, Targeting protein neddylation for cancer therapy. *Adv. Exp. Med. Biol.* **1217**, 297–315 (2020).
48. M. J. Emanuele *et al.*, Global identification of modular cullin-RING ligase substrates. *Cell* **147**, 459–474 (2011).
49. H. Liao *et al.*, Quantitative proteomic analysis of cellular protein modulation upon inhibition of the NEDD8-activating enzyme by MLN4924. *Mol. Cell. Proteomics* **10**, 009183 (2011).
50. Y. Zhao, M. A. Morgan, Y. Sun, Targeting neddylation pathways to inactivate cullin-RING ligases for anticancer therapy. *Antioxid. Redox Signal.* **21**, 2383–2400 (2014).
51. M. Melixetian *et al.*, Loss of geminin induces rereplication in the presence of functional p53. *J. Cell Biol.* **165**, 473–482 (2004).
52. Y. Kim, E. T. Kipreos, Cdt1 degradation to prevent DNA re-replication: Conserved and non-conserved pathways. *Cell Div.* **2**, 18 (2007).
53. W. Zhu, M. L. Depamphilis, Selective killing of cancer cells by suppression of geminin activity. *Cancer Res.* **69**, 4870–4877 (2009).
54. J. J. Miller *et al.*, Emi1 stably binds and inhibits the anaphase-promoting complex/cyclosome as a pseudosubstrate inhibitor. *Genes Dev.* **20**, 2410–2420 (2006).
55. D. Guardavaccaro *et al.*, Control of meiotic and mitotic progression by the F box protein β-Trcp1 in vivo. *Dev. Cell* **4**, 799–812 (2003).
56. F. Margottin-Goguet *et al.*, Prophase destruction of Emi1 by the SCF(betaTrCP/Slimb) ubiquitin ligase activates the anaphase promoting complex to allow progression beyond prometaphase. *Dev. Cell* **4**, 813–826 (2003).
57. A. Marzio *et al.*, The F-box domain-dependent activity of EMI1 regulates PARPi sensitivity in triple-negative breast cancers. *Mol. Cell* **73**, 224–237.e6 (2019).
58. S. I. Houston *et al.*, Catalytic function of the PR-Set7 histone H4 lysine 20 monomethyltransferase is essential for mitotic entry and genomic stability. *J. Biol. Chem.* **283**, 19478–19488 (2008).
59. J. Huh, H. Piwnica-Worms, Targets CHK1 for PCNA-independent destruction. *Mol. Cell. Biol.* **33**, 213–226 (2013).
60. C. M. Lovly, L. Yan, C. E. Ryan, S. Takada, H. Piwnica-Worms, Regulation of Chk2 ubiquitination and signaling through autophosphorylation of serine 379. *Mol. Cell. Biol.* **28**, 5874–5885 (2008).
61. Y. W. Zhang *et al.*, The F box protein Fbx6 regulates Chk1 stability and cellular sensitivity to replication stress. *Mol. Cell* **35**, 442–453 (2009).
62. P. Nghiem, P. K. Park, Y. S. Kim Ys, B. N. Desai, S. L. Schreiber, ATR is not required for p53 activation but synergizes with p53 in the replication checkpoint. *J. Biol. Chem.* **277**, 4428–4434 (2002).
63. R. T. Abraham, Cell cycle checkpoint signaling through the ATM and ATR kinases. *Genes Dev.* **15**, 2177–2196 (2001).
64. J. Yu, S. Tiwari, P. Steiner, L. Zhang, Differential apoptotic response to the proteasome inhibitor Bortezomib [VELCADE, PS-341] in Bax-deficient and p21-deficient colon cancer cells. *Cancer Biol. Ther.* **2**, 694–699 (2003).
65. J. A. Wohlschlegel *et al.*, Inhibition of eukaryotic DNA replication by geminin binding to Cdt1. *Science* **290**, 2309–2312 (2000).
66. J. Y. Hsu, J. D. R. Reimann, C. S. Sørensen, J. Lukas, P. K. Jackson, E2F-dependent accumulation of hEmi1 regulates S phase entry by inhibiting APC(Cdh1). *Nat. Cell Biol.* **4**, 358–366 (2002).
67. J. Hu, C. M. McCall, T. Ohta, Y. Xiong, Targeted ubiquitination of CDT1 by the DDB1-CUL4A-ROC1 ligase in response to DNA damage. *Nat. Cell Biol.* **6**, 1003–1009 (2004).
68. H. Nishitani *et al.*, Two E3 ubiquitin ligases, SCF-Skp2 and DDB1-Cul4, target human Cdt1 for proteolysis. *EMBO J.* **25**, 1126–1136 (2006).
69. K. Nishioka *et al.*, PR-Set7 is a nucleosome-specific methyltransferase that modifies lysine 20 of histone H4 and is associated with silent chromatin. *Mol. Cell* **9**, 1201–1213 (2002).
70. R. C. Centore *et al.*, CRL4(Cdt2)-mediated destruction of the histone methyltransferase Set8 prevents premature chromatin compaction in S phase. *Mol. Cell* **40**, 22–33 (2010).
71. T. Abbas *et al.*, CRL4(Cdt2) regulates cell proliferation and histone gene expression by targeting PR-Set7/Set8 for degradation. *Mol. Cell* **40**, 9–21 (2010).
72. M. Tardat *et al.*, The histone H4 Lys 20 methyltransferase PR-Set7 regulates replication origins in mammalian cells. *Nat. Cell Biol.* **12**, 1086–1093 (2010).
73. D. B. Beck *et al.*, The role of PR-Set7 in replication licensing depends on Suv4-20h. *Genes Dev.* **26**, 2580–2589 (2012).
74. A. Vassilev *et al.*, Identification of genes that are essential to restrict genome duplication to once per cell division. *Oncotarget* **7**, 34956–34976 (2016).
75. M. Jost *et al.*, Combined CRISPRi/a-based chemical genetic screens reveal that rigosertib is a microtubule-destabilizing agent. *Mol. Cell* **68**, 210–223.e6 (2017).
76. L. A. Gilbert *et al.*, Genome-scale CRISPR-mediated control of gene repression and activation. *Cell* **159**, 647–661 (2014).
77. A. Ianevski, A. K. Giri, T. Aittokallio, SynergyFinder 2.0: Visual analytics of multi-drug combination synergies. *Nucleic Acids Res.* **48** (W1), W488–W493 (2020).
78. B. Lomenick, S. D. Garbis, CSN5i-3 induces degradation of selective CRL substrate receptors and accumulation of CRL substrates. ProteomeXchange Consortium. http://proteomecentral.proteomexchange.org/cgi/GetDataset?ID=PXD027862. Accessed 8 November 2021.